Cable Fault Location in a DC Microgrid Using Current Injection Technique

Rabindra Mohanty, *Student Member, IEEE*
Electrical Engineering Department
Indian Institute of Technology
Kharagpur, India-721302

A. K. Pradhan, *Senior Member, IEEE*
Electrical Engineering Department
Indian Institute of Technology
Kharagpur, India-721302

***Abstract*—The idea of accurate fault location in distribution system expedites maintenance process, quick restoration and shorten the power outage duration. In DC microgrid, an existing fault location technique that assumes the natural frequency of the system is equal to damped resonant frequency of probe current supplied by probe power unit (PPU) evidences significant error in calculation of fault location. To estimate all possible location of line fault in low voltage DC microgrids, a portable current injection kit (CIK) is proposed in this paper. Calculating attenuation and damping frequency of the injected current the fault distance is obtained. The validity of the proposed method is tested considering high fault resistance, different fault types and radial and looped network topologies. Using MATLAB, the performance studies of the proposed fault location algorithm have been carried out through detailed simulations and more accuracy is evidenced.**

***Index Terms*—Low voltage DC microgrid, Fault distance, DC transient, damping frequency, attenuation constant.**

NOMENCLATURE

R	resistance of injection kit circuit with faulted path
L	inductance of injection kit circuit with faulted path
R_1	line resistance to fault location
L_1	line inductance to fault location
R_f	fault resistance
L_p	is the injection kit inductance
C_p	is the injection kit capacitance
R_u	resistance of the line per unit length
L_u	inductance of the line per unit length
d	distance to the fault location
l	overall line distance length
$i_p(t)$	injection kit current
α	attenuation
ζ	damping co-efficient
ω_n	natural frequency
ω_d	damping frequency

I. INTRODUCTION

LOCATING fault by traditional method in a distribution system with several branches is difficult. The strength of accurate fault location leads to advantages such as expeditious maintenance, rapid restoration and, hence, power outage duration minimization [1]. One of the features of advanced DC system is to use power electronic converters to optimize power flow, power quality, and the size and weight of the distribution equipment. During fault, the current is limited due to presence of power electronic devices up to some extend that leads to difficulty in estimating fault location operation [2], [3]. The most common fault location methods are based on impedance measurement and traveling wave [4]. Traditional distance protection is impedance based measurement at power frequency (50 Hz), this only has an accuracy of a few kilometers and so this is not suitable for distribution systems [5]. In [6]–[9], fault location technique is proposed based on reflected wave detection and discrimination which is an issue in case of close-in faults. For multi-terminal DC (MTDC) system, a traveling wave based fault location method is described in [10]. In such system, the limitation is due to variations of the shortest paths to the different detectors from the fault location point. Traveling wave and time-domain based fault location algorithms are used in high voltage DC (HVDC) transmission line. Fault generated traveling wave takes time for its propagation in the transmission line depending upon the fault position. Moreover, the accuracy of such methods depends on the accurate detection of the surge arrival time and requires high performance data acquisition equipment [11], [12].

DC distributed system is a new concept in electric power system. The growth of distributed energy resources (DERs) and the DC loads increase the number of branches of DC distributed networks and make it difficult to accurately locate a DC line fault [1], [13], [14]. The traditional fault location methods in high voltage DC network often use the natural frequency based fault location [15]. Active impedance estimation (AIE) approach is applied in marine DC power system [16]. Recently, noniterative fault-location technique using PPU, is proposed for low voltage DC microgrid [17]. However, damping coefficient (ζ) of current response id not considered in here. Furthermore, the assumption of natural frequency of the system is equal to damped frequency of current response incorporates the error in fault distance calculation.

In this paper, a new method is proposed to ac-

978-1-4799-5141-3/14/$31.00

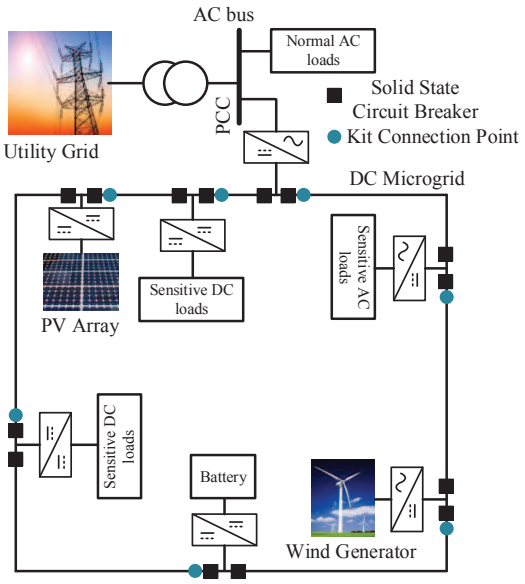

Fig. 1. DC microgrid with CIK connection point

curately locate a fault in DC line using attenuation constant (α) in damped injected current response. The damping coefficient is a function of fault resistance and therefore, it leads to inaccuracy if neglected. Using fast fourier transform (FFT) algorithm, the damped resonant frequency is obtained from sampled current data. The attenuation constant is calculated from the peak values of underdamped injected current response. This method does not require online voltage or current data to calculate the fault, hence this improves the accuracy and more economical. The accuracy and effectiveness of the method have been tested and found to be more accurate.

This paper is divided into five sections. Section I is devoted to introduction. In section II, low voltage DC microgrid is briefly discussed. The proposed fault location technique is explained in section III, simulation results including comparison study with the method [17] are given in section IV. The overall conclusions are given in section V.

II. Low Voltage DC Microgrid

Renewable energy sources like photo-voltaic array. fuel cell and storage devides are inherently producing DC power. In compatible to that, most of the sensitive electronic loads like computers, mobiles and fan, LEDs, electric vehicles consume DC. DC bus microgrid provides a platform for balance of such generation and demand with higher economy, efficiency and reliability. The reduction of AC-DC-AC conversion stages enhances the efficiency and minimizes the cost in DC distribution system [13].

Moreover, for same cable DC can deliver $\sqrt{2}$ times more power than AC. This is because, the peak voltage of the DC system is same as rms and that of AC system id $\sqrt{2}$ times more. DC systems do not experience the skin effect and corona loss. Hence, DC system utilizes the entire cable that leads decrease in losses [18], [19]. DC microgrid can be operated either in grid connected mode or islanded mode. In case demand of microgrid exceeds its generation, the extra power flows from grid and reverse power flow occurs for higher generation compared to demand in microgrid. A low voltage DC microgrid system is shown in Fig. 1. The microgrid is operated in grid connected mode and consists of sources like PV array and wind generator. Both AC and DC type loads are considered in the system. Loads are connected through DC-DC or AC-DC converters to the DC bus.

III. Proposed Fault Location Method

The point of connection of CIK in the DC system is shown in Fig. 1. and the internal circuit diagram is shown in Fig. 2 The CIK consists of a capacitor, an

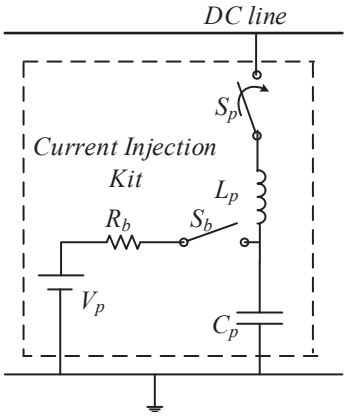

Fig. 2. Internal circuit diagram of CIK

inductor, a battery and switches. The battery injects a current in the kit circuit through faulted path. The energy stored in the kit being finite, the injected current will be small and remains for a period only.

A. Modeling of CIK with faulted section

Immediately after the isolation of faulted line segment (l), an RLC loop is formed with CIK along with the fault path as shown in Fig. 3.

The instant, when S_p is opened and S_{pf} is closed, the equation of injected current is as follows:

$$\frac{\mathrm{d}^2 i_p(t)}{\mathrm{d}t^2} + \frac{R}{L}\frac{\mathrm{d}i_p(t)}{\mathrm{d}t} + \frac{1}{LC} i_p(t) = 0 \qquad (1)$$

Let R_d and L_d be the resistance and the inductance of the line up to fault. With R_f be the fault resistance, the equivalent resistance R of the fault path is the sum of R_d and R_f. L_p and C_p are the inductance and capacitance of the CIK respectively. The equivalent inductance of the fault path L is the sum of L_d and L_p. The line charging capacitance is small compared to the kit capacitance and is neglected. The equivalent capacitance of the fault path is thus C_p.

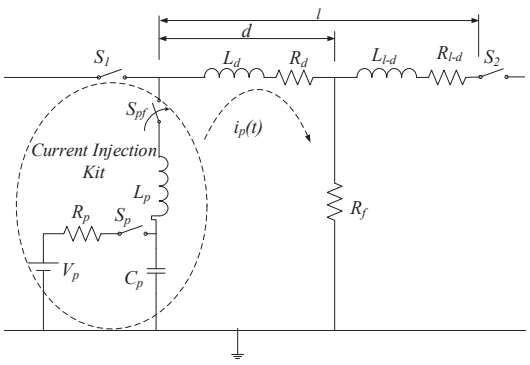

Fig. 3. Equivalent circuit of CIK with faulted line

As solution of (1), the injected current $i_p(t)$ can be written as,

$$i_p(t) = K_1 e^{-\alpha t} cos(\omega_d t) + K_2 e^{-\alpha t} sin(\omega_d t) \quad (2)$$

where, ω_d and α are the damped resonant frequency and attenuation of the injected current. The constants K_1 and K_2 can be found out by initial conditions of injected current and its differential. The RLC circuit with no driving voltage source, provides zero-input response. Thus for the circuit, the attenuation, $\alpha = R/(2L)$.

B. Formulation of attenuation constant (α)

The CIK and faulted path upto fault location formed a series RLC circuit. The injected current response in this aforementioned path is underdamped one and is shown in Fig. III-B. The positive peak of the injected current is a function of attenuation constant and time [14]. This can be expressed as

$$K_{t1} = e^{-\alpha n_1 \Delta t} = e^{-\alpha t_1} \quad (3)$$

$$K_{t2} = e^{-\alpha n_2 \Delta t} = e^{-\alpha t_2} \quad (4)$$

where Δt is the sampling interval. Fault location and resistance both being unknown, to find α, two consecutive positive peaks of exponentially decaying sinusoidal injected current are considered. Every two

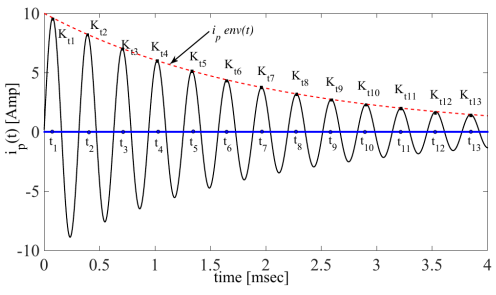

Fig. 4. Injected current response; $t[1]$,$t[2]$... are instances of positive peaks and K_{t1},K_{t2}... are the peak positive values

consecutive peaks give one attenuation and the final attenuation is the mean of the calculated attenuations as follows,

$$\alpha_1 = \frac{ln\ K_{t_1} - ln\ K_{t_2}}{t_2 - t_1} \quad (5)$$

and

$$\alpha = \frac{\sum_{i=1}^{n} \alpha_i}{n} \quad (6)$$

where, t_1 and t_2 are the instances at which peak magnitudes of damped injected current achieved at first and second times respectively, K_{t_1}, K_{t_2} are the peak magnitudes of injected current and n is the total number of samples.

The damped resonant frequency of injected current is

$$\omega_d = \sqrt{\omega_n^2 - \alpha^2} = \omega_n \sqrt{1 - \zeta^2} \quad (7)$$

where, $\omega_n = \frac{1}{\sqrt{(L_p + L_d)C_p}}$.

The damping coefficient becomes,

$$\zeta = \frac{\alpha}{\omega_n} = \frac{R}{2}\sqrt{\frac{C_p}{L}} \quad (8)$$

The current response in the kit RLC circuit is exponential decaying sinusoidal function,

$$i_p(t) = K e^{-\alpha t} sin(\omega_d t) \quad (9)$$

C. Fault distance formulation

Probe capacitance C_p, kit inductance L_p and line inductance per unit length L_u are known. Being the inductance of the faulted path is unknown, the natural frequency response also not known. This can be calculated as

$$\omega_n^2 = \omega_d^2 + \alpha^2 \quad (10)$$

$\omega_n = \frac{1}{\sqrt{(L_p + L_u d)C_p}}$. Thus the fault location d can be calculated as

$$d = \frac{1 - L_p(\omega_d^2 + \alpha^2)C_p}{L_u(\omega_d^2 + \alpha^2)C_p} \quad (11)$$

The absolute % error ϵ with and without considering attenuation are calculated and compared using the relation,

$$\epsilon = \left| \frac{d_{cal} - d_{act}}{d_{act}} \right| \times 100 \quad (12)$$

where, d_{cal} and d_{act} are the calculated and actual fault locations, respectively. The percentage error reduction is calculated as $\epsilon_{red} = \{(\epsilon - \epsilon_\alpha)/\epsilon\} \times 100$, where, ϵ_α corresponds to $\%error$ considering α and ϵ without α consideration.

D. CIK connection for different fault type

Line-to-ground faults are most common for under ground cable or line in distribution system. The CIK has two terminal for connecting to lines or ground. After isolation of faulted segment, one terminal is connected to the faulted line and other one connected to ground. With such connection, for ground fault the path is closed and current flows. In case of line-to-line fault, such connection of CIK does not provide a

close path for current and operator can not find current response. For such fault type, the ground point of CIK must be connected to other line of the DC system. This provides a close path for current and fault distance can be obtained using proposed algorithm.

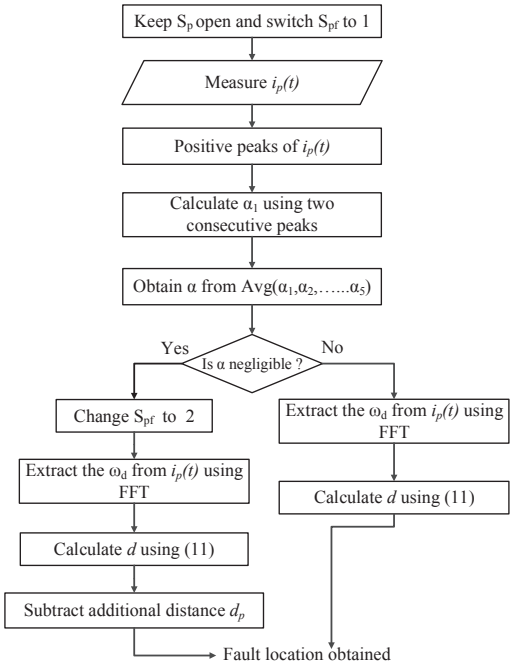

Fig. 4. Flow diagram of proposed fault location algorithm

The flowchart of proposed algorithm is shown in Fig. 4. Initially switch S_{pf} is closed to position 1 and S_p is kept open as shown in Fig. 3. The current injected to the faulted path $i_p(t)$ is measured. Subsequently ω_d is obtained using FFT and α is calculated from the positive peaks of $i_p(t)$. Using (11), fault distance is calculated. For negligible α, the position of S_{pf} will be changed to 2 which results in inclusion of additional length to introduce attenuation for ease calculation of fault distance.

IV. Simulation Results

Using MATLAB, the simulation results have been obtained including different fault resistances and varying fault distances in the 2 km line segment in the DC microgrid of Fig. 1. The percentage error is calculated for different fault distances and fault resistances. It is seen that the error by the proposed method(considering α) is reduced significantly compared to the error considering natural frequency close to the damped resonant frequency [17]. For solid ground fault i.e. $R_f = 0$, the error calculated considering attenuation emulates that of the case by neglecting α. In Table IV, the percentage error of fault location considering α (ϵ_α) is compared with the method in [17] without considering α (ϵ).For all cases with different fault resistances and fault locations the error with proposed method is lesser than the available method. Using

TABLE I
Simulation Parameter [13]

Resistance per km	121 mΩ/km
Inductance per km	0.232 mH/km
Line length	2 km
Fault location	0-100%
Probe capacitance	27 μF
Probe inductance	657 μH

the aforementioned simulation parameters in Table I for line and CIK, the fault location for different fault position and resistances are calculated with and without considering attenuation.

A. Fault location calculation considering α

In low voltage DC microgrid system, the fault resistance of 0.5 Ω is considered as higher one as in [17], however, in this paper, we have accounted it to a maximum possibilities as 2 Ω for high fault sensitivity analysis. The percentage error in fault location is calculated for different fault resistances and locations. Table II shows the percentage error in case of attenuation considered. The calculated error is

TABLE II
Fault location calculated considering attenuation for different fault resistances and locations

	Fault Resistance (in Ω)				
	0	0.5	1.0	1.5	2.0
d (%)	$\%\epsilon_\alpha$	$\%\epsilon_\alpha$	$\%\epsilon_\alpha$	$\%\epsilon_\alpha$	$\%\epsilon_\alpha$
20	0.287	0.329	1.779	3.487	6.608
40	0.049	0.203	0.835	1.942	3.526
50	0.147	0.33	0.607	1.864	2.763
60	0.114	0.093	0.884	1.383	2.463
80	0.152	0.092	0.555	1.239	2.142
100	0.003	0.272	0.372	1.192	1.836

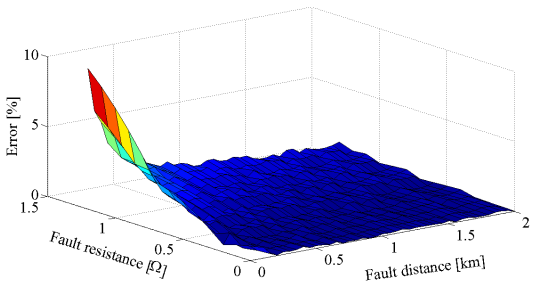

Fig. 5. Percentage error in fault location without considering attenuation

represented in three dimensional surface plot as shown in Fig. 5. The proposed method is found more accurate with high fault resistance and towards the end of the line compared to [17].

B. Fault location calculation without α

The percentage error in fault location, not considering attenuation is listed in Table III and found prominent error because of not accounting resistance of the series RLC faulted path from kit to fault position. Fig. 6 shows the percentage error with respect to different fault resistances and locations.

TABLE III
FAULT LOCATION CALCULATED WITHOUT CONSIDERING ATTENUATION FOR DIFFERENT FAULT RESISTANCES AND LOCATIONS

	Fault Resistance (in Ω)				
	0	0.5	1.0	1.5	2.0
d (%)	%ϵ	%ϵ	%ϵ	%ϵ	%ϵ
20	0.283	0.856	3.735	7.843	7.843
40	0.057	0.514	1.897	4.236	7.586
50	0.157	0.600	1.492	3.753	6.059
60	0.102	0.335	1.655	2.992	5.258
80	0.136	0.301	1.182	2.518	4.329
100	0.017	0.464	0.913	2.273	3.654

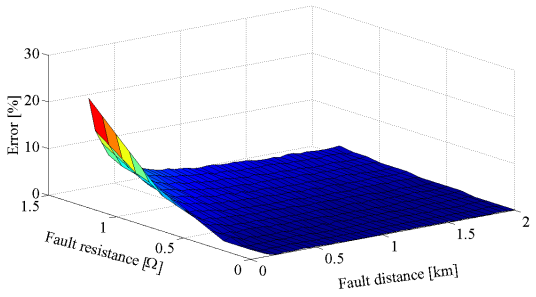

Fig. 6. Percentage error in fault location without considering attenuation

TABLE IV
PERCENTAGE ERROR COMPARISON BETWEEN PROPOSED METHOD AND THE METHOD IN [17].

	Fault Resistance (in Ω)							
	0.5		1.0		1.5		2.0	
l(%)	ϵ	ϵ_α	ϵ	ϵ_α	ϵ	ϵ_α	ϵ	ϵ_α
20	0.856	0.329	3.735	1.779	7.843	3.487	7.852	6.608
40	0.514	0.203	1.897	0.835	4.236	1.942	7.586	3.526
50	0.600	0.330	1.492	0.607	3.753	1.864	6.059	2.763
60	0.335	0.093	1.655	0.884	2.992	1.383	5.258	2.463
80	0.301	0.092	1.182	0.555	2.518	1.239	4.329	2.142
100	0.464	0.272	0.913	0.372	2.273	1.192	3.654	1.836

Fig. 7 shows the plot for ϵ_{red} for different fault resistances and fault distances where it is clearly observed that the method reduces the estimation error compared to method in [17] with the presence of fault resistance.

The consideration of ζ including kit, line and fault resistance in calculation, the injected current response is well captured because of significant damping and

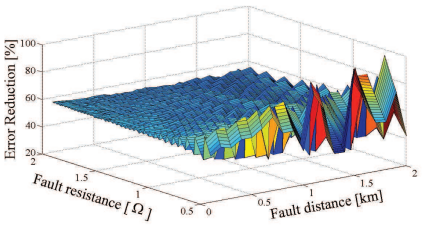

Fig. 7. Percentage error reduction in fault location by the proposed method compared to method in [17].

hence, ω_d can be easily calculated by fast fourier transform (FFT) algorithm. The injected current response $i_p(t)$ is sampled at the rate of 2kHz.

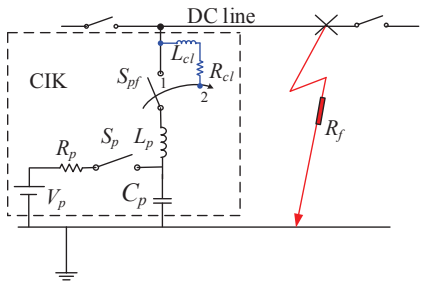

Fig. 8. Equivalent circuit of PPU for close fault

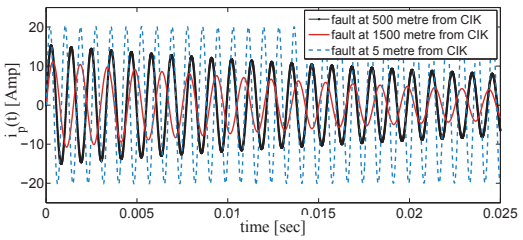

(a)

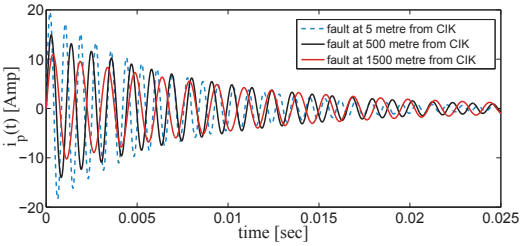

(b)

Fig. 9. Probe current response in (a) fault close to PPU and (b) fault close to PPU with inclusion of resistance R_{cl} in Fig. 8

C. Performance during a fault close to CIK

A fault close to CIK leads negligible attenuation in the current response. The validity of proposed algorithm is tested for a fault very close to kit. A fault is simulated at a distance of 5 m from CIK and α is calculated. This results the value of α to

be negligible, this is because two consecutive positive peaks of $i_p(t)$ are almost of same value. The injected current responses for fault at 5 m, 500 m and 1500 m from CIK in a 2 km line segment are shown in Fig. 9a. It is shown that the damping is significant in case of larger fault distance such as for 500 m and 1500 m. But the challenge is when a fault occurs close to CIK. For such a situation, to provide a significant damping, an additional distance (d_p) in terms of resistance and inductance is included externally. To achieve this the position of switch S_{pf} can be changed to 2 as shown in Fig. 8. The equivalent resistance and inductance values of additional length of line are represented as R_{cl} and L_{cl} respectively. The ranges for R_{cl} between 60 $m\Omega$ to 100 $m\Omega$ and for L_{cl} between 0.48 mH to 0.8 mH which corresponds to a length of 500 m to 800 m are good enough for the system. The injected current responses for this case are given in Fig. 9b which shows that attenuation can easily be calculated for a very close fault to CIK. The accuracy for a fault at 5 m from CIK is found to be 99.74%. Finally, the actual fault distance is obtained by subtracting the additional length from the calculated one.

V. Conclusion

In this work, a new method is proposed for fault location in DC system with higher accuracy. A relationship is established among damping frequency, attenuation constant and fault distance. Considering attenuation, calculation of fault location is performed and a comparative study has been done. It is noticed that the proposed method is more accurate for different fault resistances. Also the performance of the method is checked for a fault close to CIK and the fault distant is calculated accurately. The algorithm presented in this paper is expected to be a promising fault location method in DC microgrid system.

ACKNOWLEDGMENT

We would like to thank the Department of Science and Technology (DST), New Delhi, India for sponsoring the Indo-UK joint project (DST/RCUK/SEGES/2012/09(G), 29-09-2014) through which the work is being carried out.

References

[1] J. Ren, S. S. Venkat, and E. Sortomme, "An accurate synchrophasor based fault location method for emerging distribution systems," *IEEE Trans. Power Del.*, vol. 29, pp. 297–298, Feb. 2014.

[2] T. Ericsen, N. Hingorani, and Y. Khersonsky, "Power electronics and future marine electrical systems," *Industry Applications, IEEE Transactions on*, vol. 42, pp. 155–163, Jan 2006.

[3] R. Cuzner and G. Venkataramanan, "The status of dc microgrid protection," in *Industry Applications Society Annual Meeting, 2008. IAS '08. IEEE*, pp. 1–8, Oct 2008.

[4] A. Dalcastagne, S. Noceti Filho, H. Zurn, and R. Seara, "An iterative two-terminal fault-location method based on unsynchronized phasors," *Power Delivery, IEEE Transactions on*, vol. 23, pp. 2318–2329, Oct 2008.

[5] C. Christopoulos and A.Wright, *Elect. Power Syst. Protect. 2nd ed.* New York: Springer, 1999.

[6] M. Ando, E. O. Schweitzer, and R. A. Baker, "Development and field data evaluation of single end fault locator for two-terminal hvdc transmission lines-part 2 : algorithm and evaluation," *IEEE Transactions on Power Apparatus and Systems*, vol. PAS-104, pp. 3531–3537, Dec 1985.

[7] D. Spoor and J. G. Zhu, "Improved single-ended traveling-wave fault-location algorithm based on experience with conventional substation transducers," *IEEE Trans. Power Del.*, vol. 21, pp. 1714–1720, July 2006.

[8] M. B. Dewe, S. Sankar, and J. Arrillaga, "The application of satellite time references to hvdc fault location," *IEEE Trans. Power Del.*, vol. 8, pp. 1295–1302, July 1993.

[9] P. Jafarian and M. Sanaye-Pasand, "A traveling-wave-based protection technique using wavelet/pca analysis," *IEEE Trans. Power Del.*, vol. 25, pp. 588–599, April 2010.

[10] S. Azizi, M. Sanaye-Pasand, M. Abedini, and A. Hassani, "A traveling-wave-based methodology for wide area fault location in multiterminal dc systems," *IEEE Trans. Power Del.*, vol. 29, pp. 2552–2560, Dec 2014.

[11] Z. you He, K. Liao, X. peng Li, S. Lin, J. wei Yang, and R. kun Mai, "Natural frequency-based line fault location in hvdc lines," *Power Delivery, IEEE Transactions on*, vol. 29, pp. 851–859, April 2014.

[12] A. Borghetti, M. Bosetti, C. Nucci, M. Paolone, and A. Abur, "Integrated use of time-frequency wavelet decompositions for fault location in distribution networks: Theory and experimental validation," *Power Delivery, IEEE Transactions on*, vol. 25, pp. 3139–3146, Oct 2010.

[13] J.-D. Park and J. Candelaria, "Fault detection and isolation in low-voltage dc-bus microgrid," *IEEE Trans. Power Del.*, vol. 28, pp. 779–787, Jan. 2013.

[14] R. Mohanty, U. S. M. Balaji, and A. K. Pradhan, "An accurate noniterative fault-location technique for low-voltage dc microgrid," *IEEE Trans. Power Del.*, vol. 31, pp. 475–481, April 2016.

[15] K. Liao, Z. He, and X. Li, "A fault location method based on traveling wave natural frequency used on uhvdc transmission lines," *IEEE Int. conf. on ICECE*, pp. 5652–5655, 2011.

[16] E. Christopher, M. Sumner, and D. Thomas, "Fault location in a zonal dc marine power system using active impedance estimation," *IEEE Trans. Power Del.*, vol. 49, no. 2, pp. 860–865, 2013.

[17] J.-D. Park, J. Candelaria, L. Ma, and K. Dunn, "DC ring-bus microgrid fault protection and identification of fault location," *IEEE Trans. Power Del.*, vol. 28, pp. 2574–2584, May 2013.

[18] M. Saeedifard, M. Graovac, R. F. Dias, and R. Iravani, "DC power systems: Challenges and opportunities," in *IEEE PES General Meeting*, pp. 1–7, July 2010.

[19] P. Salonen, P. Nuutinen, P. Peltoniemi, and J. Partanen, "LVDC distribution system protection: Solutions, implementation and measurements," in *Power Electronics and Applications, 2009. EPE '09. 13th European Conference on*, pp. 1–10, Sept 2009.